Published in final edited form as:
Dev Cell. 2012 February 14; 22(2): 348–362. doi:10.1016/j.devcel.2011.12.009.

Secreted VAPB/ALS8 major sperm protein domains modulate mitochondrial localization and morphology via growth cone guidance receptors

Sung Min Han[1], **Hiroshi Tsuda**[2], **Youfeng Yang**[1], **Jack Vibbert**[1], **Pauline Cottee**[1], **Se-Jin Lee**[1], **Jessica Winek**[1], **Claire Haueter**[3], **Hugo J. Bellen**[2,3,4], and **Michael A. Miller**[1,*]

[1]Department of Cell Biology, University of Alabama School of Medicine, Birmingham, Alabama

[2]Department of Molecular and Human Genetics, Baylor College of Medicine, Houston, Texas 77030

[3]Howard Hughes Medical Institute, Baylor College of Medicine, Houston, Texas 77030

[4]Program in Developmental Biology, Baylor College of Medicine, Houston, Texas 77030

SUMMARY

The VAPB/ALS8 major sperm protein domain (vMSP) is implicated in amyotrophic lateral sclerosis and spinal muscular atrophy, yet its function in the nervous system is not well understood. In *C. elegans* and *Drosophila*, the vMSP is cleaved from its transmembrane anchor and secreted in a cell type-specific fashion. We show that vMSPs secreted by neurons act on Lar-like protein-tyrosine phosphatase and Roundabout growth cone guidance receptors expressed in striated muscle. This signaling pathway promotes Arp2/3-dependent actin remodeling and mitochondrial localization to actin-rich muscle I-bands. *C. elegans* VAPB mutants have mitochondrial localization, morphology, mobility, and fission/fusion defects that are suppressed by Lar-like receptor or Arp2/3 inactivation. Hence, growth cone guidance receptor pathways that remodel the actin cytoskeleton have unanticipated effects on mitochondrial dynamics. We propose that neurons secrete vMSPs to promote striated muscle energy production and metabolism, in part through the regulation of mitochondrial localization and function.

Keywords

ALS; SMA; VAPB; MSP; *Drosophila*; *C. elegans*; Eph receptors; Roundabout receptors; Lar receptors; mitochondria; fission; fusion; actin

INTRODUCTION

Mitochondria are obligate endosymbionts that generate ATP for cellular energy through oxidative phosphorylation and play central roles in metabolism, calcium homeostasis, and apoptosis (Parekh, 2003; Suen et al., 2008). They are often distributed non-randomly in

*Corresponding author: Michael A. Miller, Tel: 205-996-2096, Fax: 205-934-7029, mamiller@uab.edu.

SUPPLEMENTAL DATA

Supplemental Data include 5 figures, 2 Tables, 4 movies, supplemental experimental procedures, and references.

differentiated cells like neurons and muscle, presumably to provide energy to regions high in metabolic demand. In neurons, mitochondria are enriched at synapses (Hollenbeck and Saxton, 2005), whereas in mammalian skeletal muscle, mitochondria are positioned in pairs near the I-bands (Vendelin et al., 2005). Motor proteins that move along microtubules drive mitochondrial transport over long distances (Hollenbeck and Saxton, 2005). However, the actin cytoskeleton can facilitate short-range mitochondrial movement and docking of mitochondria to specific sites (Boldogh and Pon, 2007; Pathak et al., 2010). In chicken sensory neuron cultures, Nerve Growth Factor-conjugated beads promote mitochondrial accumulation and docking by a mechanism dependent on F-actin (Chada and Hollenbeck, 2004). These data raise the possibility that growth factors may affect mitochondrial localization *in vivo*.

The VAPs (VAMP/synaptobrevin-associated proteins) comprise a highly conserved protein family with an N-terminal MSP (major sperm protein) domain, a coiled-coil motif, and transmembrane-spanning region anchored in endoplasmic reticulum (ER) membranes. The ~120 amino acid MSP domain is named after *C. elegans* MSPs, which function as secreted ligands that induce oocyte maturation and ovarian muscle contraction (Han et al., 2010; Miller et al., 2001). MSPs also have an intracellular cytoskeletal function, but this function is independent of actin and myosin, depends upon MSP polymerization into filaments, and is not conserved in VAPs (Bottino et al., 2002; Han et al., 2010; Lev et al., 2008). VAPs have been implicated in diverse processes, including regulation of lipid transport, ER morphology, and membrane trafficking (Lev et al., 2008). In addition, VAPs and MSPs have a conserved function as a secreted signaling molecule (Tsuda et al., 2008). We have shown that VAP MSP domains (vMSPs) are cleaved from the transmembrane domain and secreted into the extracellular environment, where they bind to Eph Receptors (EphRs) and other unidentified receptors (Miller et al., 2003; Tsuda et al., 2008). The secretion mechanism appears to be unconventional and cell-type specific.

A P56S mutation in the human VAPB MSP domain causes amyotrophic lateral sclerosis (ALS) and late-onset spinal muscular atrophy (SMA), two neuropathies characterized by progressive muscle atrophy and motor neuron degeneration (Funke et al., 2010; Millecamps et al., 2010; Nishimura et al., 2004). VAP^{P56S} causes VAP ubiquitination, recruitment of wild-type and mutant VAPs to cytoplasmic inclusions (Teuling et al., 2007; Tsuda et al., 2008), and impaired MSP domain secretion (Tsuda et al., 2008). VAPB levels are reduced in sporadic ALS patients, *sod1* mutant mice, and ALS8 patient motor neurons derived from induced pluripotent stems cells, suggesting that VAPB plays a widespread role in pathogenesis (Anagnostou et al., 2010; Mitne-Neto et al., 2011; Teuling et al., 2007).

Here, we present evidence that MSP domains comprise a conserved ligand class that modulates mitochondrial localization and morphology in muscle and oocytes. Neurons secrete vMSPs to promote mitochondrial docking at actin-rich I-bands of *C. elegans* striated muscle. vMSPs transduce signals through muscle Roundabout and Lar-like receptors that modulate the actin-related protein 2/3 (Arp2/3) complex. VAP loss causes aberrant Lar receptor and Arp2/3 activity that displaces mitochondria from I-bands, influences the fission/fusion balance, and decreases transmembrane potential. We propose that neurons secrete vMSPs to promote mitochondrial localization and function important for energy metabolism in muscles.

RESULTS

VAP loss causes muscle mitochondrial defects in *Drosophila* and *C. elegans*

We previously documented that neuronal overexpression of dVAP, a *Drosophila* VAPB homolog (Pennetta et al., 2002), caused myofibrillar defects in the indirect flight muscle

(IFM) of adult flies (Tsuda et al., 2008). This defect could be suppressed by Eph receptor knockout, suggesting that neurons secrete the dVAP MSP domain. The IFMs are massive and provide most of the energy needed for flight. To test whether VAP loss affects muscle, we examined the IFM in wild-type and *dvap* null mutant flies using transmission electron microscopy (TEM). In wild-type adults, TEM shows that the mitochondria are arranged in columns between the myofibrils (Fig. 1A). In contrast, most mitochondria in *dvap* null mutant muscle are small and have abnormal cristae, whereas others are larger and have vacuole-like structures [Fig. 1A; 84% of the mitochondria lack lamellar cristae, whereas 7% are enlarged, lack electron density, and are highly aberrant (N = 123)]. The myofibrils, on the other hand, appear similar to control myofibrils. Hence, dVAP loss causes severe mitochondrial morphology defects in adult fly muscles.

Next, we examined adult *C. elegans* body wall muscle to test whether the role of VAPs (*vpr-1* in worms) is evolutionarily conserved. Mitochondria were visualized in live muscle by expressing mitochondrial matrix-targeted GFP (mitoGFP) under control of the *myo-3* muscle promoter, as well as by feeding worms the dyes Mitotracker CMXRos and Rhodamine 6g. In wild-type adults, muscle mitochondria form largely unbranched tubules within the belly (Fig. 1B, C). 84.7% of these tubules in mitoGFP transgenic worms form linear arrays that are regularly spaced, correlating with the spacing between I-bands (Fig. 1C, D; Table S1, line 1). Indeed, the mitochondrial arrays overlap with the dense bodies, which occupy the middle of the I-band and appear as small bumps organized in the same orientation as the myofilaments (Fig. 1D). Identical results are observed with Mitotracker CMXRos and Rhodamine 6g. Additional support for the association of mitochondria with I-bands comes from muscle TEM cross sections (Fig. 2A).

In contrast to wild type, mitochondria in *vpr-1(tm1411)* mutants are not arranged in parallel arrays and are rarely associated with dense bodies (Fig. 1D and 1E; Table S1, lines 1 and 2). 3D microscopy indicates that mitochondria form thin and highly branched tubular networks within the muscle belly (Fig. 1E). TEM cross sections confirm that mitochondrial tubules in *vpr-1* mutant muscle are smaller in diameter than controls and mostly displaced from the myofilaments (Fig. 2B; Table S1, lines 1 and 2, $P < 0.001$). The muscle belly is expanded, in part due to abnormal actin branching (see below) and mitochondria rarely localize to I-bands. Muscle myofilaments, ER, and motor neuron positions in *vpr-1* mutants appear similar to the wild type (Fig. 2B and data not shown). Moreover, *vpr-1* mutants do not exhibit abnormal muscle ER homeostasis (S. Han and M. Miller, unpublished data). We conclude that *vpr-1* is required for formation of tubular and largely unbranched mitochondrial arrays positioned along the I-bands. Collectively, these data indicate that VAP loss in *Drosophila* and *C. elegans* causes specific defects in muscle mitochondrial morphology.

VAP mutants have interconnected mitochondrial networks

The mitochondrial tubules in *vpr-1* mutant muscle appear more fused than tubules in wild-type muscle (Fig. 1E). RNAi of the outer membrane fission mediator *drp-1* and the inner membrane fusion mediator EAT-3/OPA1 can be used to shift the fission/fusion balance in mitochondrial networks (Kanazawa et al., 2008; Labrousse et al., 1999). Shifting the balance toward fusion in wild-type animals by *drp-1* RNAi causes the formation of elongated and branched networks similar to those in *vpr-1* mutants, except that the matrix often accumulates in large aggregates (Fig. 3A). *drp-1* RNAi in *vpr-1* mutants also causes accumulation of identical aggregates. Shifting the balance toward fission in wild-type and *vpr-1* mutant animals by *eat- 3/opa1* RNAi causes mitochondrial fragmentation (Fig. 3A). These data suggest that muscle mitochondria in *vpr-1* mutants have low fission/fusion balance.

We tested whether or not the mitochondrial tubules in *vpr-1* mutants are physically connected to each other, consistent with their appearance in confocal axial scans. Fluorescence loss in photobleaching (FLIP) can be used to assess connectivity among muscle mitochondria. Our fluorescence recovery after photobleaching experiments (data not shown) and a previous study demonstrate that mitoGFP rapidly diffuses between contiguous compartments (Labrousse et al., 1999). In FLIP experiments, a mitochondrial tubule is repeatedly photobleached every 5 seconds followed by a scan of the surrounding area. Contiguous mitochondria lose fluorescence during each cycle, as mitoGFP diffuses into the bleached area. Thus, interconnected mitochondrial networks will exhibit rapid reduction in fluorescence outside of the bleached spot. To assess mitochondrial connectivity with FLIP, we used conditions that stabilize mitochondria and prevent their mobility. FLIP in control muscles causes rapid fluorescence loss in the targeted area, but the vast majority of surrounding mitochondria retain their fluorescence, even after 48 cycles (Fig. 3B, C). In 5 of 11 experiments, a single neighboring tubule lost fluorescence. The average bleached area in the 11 experiments was 7.8 μm^2, indicating that individual tubules have limited connectivity in wild-type muscle. In contrast to the wild type, FLIP in *vpr-1* mutant muscles resulted in rapid loss of fluorescence in the targeted area and numerous surrounding mitochondrial tubules within 20 seconds of photobleaching initiation (Fig. 3B, D). The average bleached area in 9 experiments was 32.6 μm2 ($P < 0.001$ compared to the control). We calculated that each *vpr-1* mutant muscle contains between 20 to 25 contiguous subpopulations of mitochondria, whereas each wild-type muscle contains more than 100 subpopulations (based on an average muscle area of 800 μm^2). Therefore, mitochondrial networks in *vpr-1* mutant muscle exhibit increased connectivity relative to networks in wild-type muscle. This increase in connectivity may be due to an increase in fusion, reduction in fission, or both.

Mitochondrial dynamics can be observed in live animals using time-lapse fluorescence microscopy. Mitochondria in wild-type muscle appear stably docked at I-bands (Video S1). Shape changes and fission gradually reduce tubule length over time during imaging. In *vpr-1* mutants, mitochondrial tubules exhibit increased mobility (Video S2) and occasionally form ring-shaped structures that join other tubules or collapse (Fig. S1A and Video S3). Tubules move at speeds between 0–2.0 μm/min, although only a fraction of tubules are mobile under our conditions. We noticed that fission sites in wild-type muscle are different than sites in *vpr-1* mutant muscle. In the control, fission primarily occurs within elongated tubules (29/29 fission events from 8 videos). However, fission rarely occurs within elongated tubules in *vpr-1* mutants (1/12 fission events from 8 videos) and instead occurs at connection sites between tubules (Video S4). We conclude that mitochondria in *vpr-1* mutants are more mobile and have different fission sites relative to mitochondria in wild-type muscle. Taken together, the results support the model that VPR-1 influences the fission/fusion balance.

VAP mutants have impaired mitochondrial function

The abnormal mitochondrial morphology in *vpr-1* mutants raises the possibility that their function is impaired. To evaluate muscle mitochondrial function, we used MitoTracker CMXRos, a fluorescent dye that concentrates in the mitochondrial matrix depending on transmembrane potential (Pendergrass et al., 2004). MitoTracker accumulation in *vpr-1* mutant muscle mitochondria is reduced compared to accumulation in controls (Fig. 3E). We found that *drp-1* RNAi could increase MitoTracker accumulation, suggesting that matrix aggregation caused by DRP-1 loss can partially restore mitochondrial transmembrane potential in *vpr-1* mutants (Fig. S1B). Importantly, this MitoTracker accumulation defect can be fully suppressed (see below), indicating that *vpr-1* mutants are not deficient in dye uptake or muscle transport.

Worms with reduced mitochondrial respiration should consume less oxygen and generate less ATP. Indeed, *vpr-1* mutants consume less oxygen than controls, whether the data are

normalized to protein content (Fig. 3F) or worm number (Fig. 3G). ATP concentration in one day old adult *vpr-1* mutants is significantly reduced compared to adult controls (Fig. 3H). We previously showed that sperm-derived MSPs promote ROS production in oocytes (Yang et al., 2010). *vpr-1* mutants are more resistant than the wild type to paraquat, which generates intracellular ROS that cause a concentration-dependent toxicity depending on endogenous ROS levels (Fig. 3I). Hence, *vpr-1* mutants have reduced ROS, which could be due to decreased production or increased breakdown. These independent metabolic assays support the hypothesis that *vpr-1* mutants have altered mitochondrial function.

Inhibition of mitochondrial electron transport chain (ETC) activity causes defects such as sluggish motility, reduced swimming rate in liquid, prolonged defecation cycle, reduced brood size, slow development, and larval arrest (Tsang and Lemire, 2003; Wong et al., 1995a). In particular, muscle-specific ETC inhibition affects motility, brood size, and possibly defecation and development rate (Durieux et al., 2011). Thus, *vpr-1* mutants should exhibit some of these defects if their mitochondria have reduced respiration, as indicated by the metabolic assays. Indeed, *vpr-1* null mutants exhibit sluggish motility, reduced swimming rate (99.7±9.4 thrashes/min for *vpr-1(tm1411)* vs. 125.3±11.8 thrashes/min for wild type; $P < 0.005$), prolonged defecation cycle (59.9±7.2s for *vpr-1(tm1411)* vs. 55.0±7.1s for wild type; $P < 0.01$), sterility, and slow development (57.7±3.9 hrs. for *vpr-1(tm1411)* vs. 42 hrs. for wild type; $P < 0.001$). We conclude that *vpr-1* mutants have defects consistent with abnormal mitochondrial function in muscle and possibly other cell types.

Secreted neuronal vMSPs modulate muscle mitochondrial position and morphology

Our previous studies showed that VAP MSP domains are secreted in a cell type-specific fashion (Tsuda et al., 2008). However, VAPs can also have cell autonomous functions. To determine the site(s) where VAPs function, we first examined *Drosophila*. Expressing dVAP in muscle of *dvap* null mutant flies using the *MHC-GAL4* driver causes 100% lethality and does not rescue *dvap* mutant defects. In contrast, expressing dVAP using neuronal drivers, including *C164-GAL4* and *Elav-GAL4*, rescues the lethality (Chai et al., 2008; Tsuda et al., 2008) and nearly 100% of muscle mitochondrial defects associated with *dvap* loss (Fig. 1A and data not shown). These data indicate that dVAP functions in a cell nonautonomous fashion, consistent with a signaling role.

Next, we examined the mechanism by which VPR-1 acts on muscle in *C. elegans*. Transgenic GFP reporters driven by upstream *vpr-1* genomic sequence show broad expression in adults, including the ventral nerve cord and body wall muscle (Fig. S2), similar to *Drosophila* dVAP. However, *vpr-1* expression in muscles using the *myo-3* promoter or intestine using the *ges-1* promoter does not affect muscle mitochondrial shape or distribution in the mutants (Figs. 1E and S1C). In contrast, *vpr-1* expression in neurons with the *unc-119* pan-neuronal promoter rescues mitochondrial morphology, distribution, and I-band position (Figs. 1E) in ~30–40% of muscles, while most remaining muscles exhibit improved phenotypes. The incomplete rescue may be due to transgene expression mosaicism, overexpression, or missing untranslated regulatory sequences, as neuronal expression in flies rescues nearly 100% of mitochondrial defects and neuron-specific VPR-1 inhibition causes mitochondrial defects in nearly all muscle (data not shown and see below). We conclude that VAPs are required in neurons to control muscle mitochondrial position and shape.

The above data are consistent with neurons secreting vMSP domains to regulate muscle mitochondria. To further test this model, we inhibited neuronal vMSP secretion in wild-type worms. The VAP^{P56S} mutation acts as a dominant negative, sequestering wild-type VAP in neuronal aggregates (Ratnaparkhi et al., 2008; Teuling et al., 2007) and preventing secretion

of the wild-type protein (Tsuda et al., 2008). Neuronal VPR-1^{P56S} overexpression causes muscle mitochondria to form thin, branched, and abnormally distributed networks within the muscle belly, similar to *vpr-1* null mutants (Fig. 1E). When we overexpressed neuronal VPR-1^{P56S} in *vpr-1* null mutants, muscle mitochondria were identical to those seen in nontransgenic *vpr-1* mutant controls. These data confirm that VPR-1^{P56S} acts as a dominant negative and support the model that neurons secrete vMSPs to regulate muscle mitochondria.

C. elegans, *Drosophila*, and mammalian VAPs are cleaved between the MSP domain and the transmembrane domain (Gkogkas et al., 2011; Tsuda et al., 2008). Previously, we documented vMSP secretion in *Drosophila* wing disc cells by expressing a dVAP fusion protein with distinct N-terminal and C-terminal tags (Tsuda et al., 2008). Only the N-terminal tag containing the MSP domain was secreted. We used a similar strategy to test whether *C. elegans* neurons secrete the VPR-1 MSP domain. mCherry was fused to the N-terminus of VPR-1 and GFP to the C-terminus and this mCherry::VPR-1::GFP fusion protein was expressed in neurons using the *unc-119* promoter (Fig. 4A). While partial co-localization of mCherry and GFP was observed in motor neuron cell bodies (and other neuron bodies), mCherry was observed within axons and in the extracellular environment (Fig. 4B–D). GFP does not co-localize with most axonal mCherry, nor does it co-localize with extracellular mCherry, indicating that the VPR-1 fusion protein is cleaved. Secreted mCherry/MSP fragments were observed at the body wall and vulval muscles (Fig. 4C, D). mCherry also accumulated in the coelemocytes, mesodermal cells that nonspecifically endocytose fluid and secreted molecules within the body cavity (data not shown) (Fares and Greenwald, 2001). Taken together, these results provide strong evidence that neurons secrete vMSPs.

An MSP receptor screen identifies SAX-3 Robo and CLR-1 Lar receptors

An important prediction based on above data is that secreted vMSPs regulate a muscle receptor pathway(s) that transduces signals to mitochondria. vMSPs bind to EphRs and other unidentified receptors (Miller et al., 2003; Tsuda et al., 2008). However, EphR loss in *C. elegans* or *Drosophila* does not influence muscle mitochondria or mitochondria-related phenotypes (data not shown), suggesting that an unknown receptor(s) mediates this signaling mechanism. We previously developed an MSP receptor identification assay based on the ability of recombinant MSP domains conjugated to fluorescein (MSP-FITC) to specifically bind to receptors expressed in oocytes (Miller et al., 2003) (Fig. S3A, B). In the worm gonad, sperm secrete MSPs to induce oocyte maturation (Fig. 5A), which involves metabolic changes (Han et al., 2010; Yang et al., 2010). Under conditions where all MSP receptor sites are occupied, MSP-FITC binding to oocytes is reduced by ~35% when the VAB-1 EphR is absent (Miller et al., 2003). The remaining binding is due to unidentified MSP domain receptors. Sperm-derived MSPs and VAP MSP domains bind to identical receptors expressed in oocytes (Miller et al., 2003; Tsuda et al., 2008). We hypothesized that both oocytes and muscle express MSP domain receptors that transduce signals to mitochondria. Support for this hypothesis comes from examining the effects of extracellular MSP addition to oocyte mitochondria. Microinjecting MSPs and human vMSPs into the extracellular spaces of spermless reproductive tracts induces a rapid transition (<15 min.) in oocyte mitochondria from ring-shaped to branched, tubular forms (Figs. 5A, 5B, and S4A–D). These shape changes, as well as MSP-induced mitochondrial transport into growing oocytes (Govindan et al., 2009; Wolke et al., 2007), are dependent on *drp-1* (Fig. S4E, F). Identical shape changes in oocyte mitochondria occur when sperm presence is manipulated through mating (Fig. 5B and S4B–D). Thus, oocytes likely express MSP receptors that rapidly regulate mitochondrial shape.

To identify MSP domain receptors important for mitochondria, we compared genome-wide DNA microarray datasets of adult hermaphrodites undergoing oogenesis to those undergoing spermatogenesis (Reinke et al., 2004). MSPs bind to oocyte plasma membranes, but not to sperm plasma membranes (Miller et al., 2003). From the top 3000 oogenesis/spermatogenesis-enriched genes, we identified 40 genes that encode cell surface receptors (Table S2). These genes are not specifically expressed in oocytes; many are also expressed in neurons and muscle. We screened RNAi clones corresponding to the 40 predicted receptors to identify clones that cause reduced MSP-FITC binding to oocytes and mitochondrial shape or positioning defects in oocytes and muscle (Table S2). The only RNAi clones that affected both MSP binding and muscle mitochondria corresponded to the SAX-3 Roundabout (Robo) and CLR-1 Lar-like (Lar) receptors (Fig. 5C, D; Table S2) (Kokel et al., 1998; Zallen et al., 1998). Analysis of *clr-1* and *sax-3* mutants confirmed that both receptors are required for MSP-FITC binding and muscle mitochondrial morphology (see below). Previous studies have shown that SAX-3 Robo and CLR-1 Lar are expressed in oocytes, motor neurons, and body wall muscle (Chang et al., 2004; Kohara, 2001; Zallen et al., 1998).

SAX-3 or CLR-1 loss causes a significant reduction in MSP-FITC binding to oocytes, similar to loss of the MSP/ephrin receptor VAB-1 (Fig. 5C, D). To test whether CLR-1 Lar or SAX-3 Robo expression is sufficient to promote MSP binding, we expressed these receptors alone and in combination in cultured HEK293 cells (Fig. 5E–G). Expressing the VAB-1 EphR in cultured cells confers increased MSP-FITC cell surface binding and rapid internalization in live cells (Miller et al., 2003). We found that CLR-1 Lar expression resulted in the same significantly increased level of MSP-FITC and vMSP-FITC binding as the VAB-1 EphR positive control, whereas Robo expression resulted in a weak increase relative to the negative control (Fig. 5E–G). However, expressing both SAX-3 Robo and CLR-1 Lar together caused a synergistic increase in MSP and vMSP binding, which could be inhibited by incubating cells with an excess of unlabelled MSP (Fig. 5E–G). These data support the model that Robo and Lar function together to promote vMSP binding. Consistent with this idea, SAX-3 and CLR-1 loss synergistically affects human vMSP binding to *C. elegans* oocytes (Fig. S3C, D). In summary, our screen identified SAX-3 Robo and CLR-1 Lar, perhaps acting via a receptor complex, as candidates for mediating VAP signaling to muscle mitochondria.

SAX-3 Robo and CLR-1 Lar function in muscle to influence mitochondria

To specifically evaluate muscle mitochondria in *sax-3* Robo and *clr-1* Lar mutants, we generated *myo-3p::mitoGFP* transgenic lines. *sax-3(ky123)* mutants have incompletely penetrant and variably expressed mitochondrial defects [63.7% of *sax-3(ky123)* muscles affected (N = 55) vs. 100% for *vpr-1* mutants [N > 400]). The affected muscles have mitochondrial networks nearly identical to *vpr-1* mutants, including abnormally positioned elongated mitochondria with excess branching (Fig. 6A; Table S1, lines 1–3). TEM cross sections of *sax-3* mutant muscle show that mitochondria are smaller in diameter than controls and mostly displaced from the I-bands, similar to *vpr-1* mutants (Fig. 2B). However, the muscle belly is less swollen than *vpr-1* mutants and not all *sax-3* mutant muscles are affected, consistent with the presence of a second vMSP receptor. The *sax-3(ky123)* mutant defects were rescued with a fosmid containing the *sax-3* genomic locus, indicating that the defects are due to loss of SAX-3 Robo (Fig. 6A). Temperature shift experiments using the *sax-3(ky200)ts* hypomorphic temperature sensitive (ts) allele indicate that *sax-3* is required postembryonically (Fig. 6A). We also tested the gene encoding the Slit ligand for SAX-3 Robo and did not detect mitochondrial defects in *slt-1(eh15)* null mutants (Fig. 6A). As *slt-1* is the only Slit homolog present in *C. elegans* (Hao et al., 2001), SAX-3

does not require Slits for regulating muscle mitochondrial morphology. Therefore, *sax-3* Robo influences muscle mitochondrial shape and positioning independent of Slit.

Next, we evaluated metabolic status in *sax-3* Robo mutants. MitoTracker CMXRos staining indicated that *sax-3(ky123)* mutants have a variably expressed transmembrane potential defect (Fig. 6B) where the more severe cases resemble *vpr-1* mutants. Adult *sax-3* mutants consumed less oxygen than controls, but contained less total protein, so the interpretation depends on the normalization method (Fig. 6C). Compared to wild-type controls, *sax-3* mutants had reduced ATP concentration (Fig. 6D), increased resistance to paraquat (Fig. 6E), and slower growth (53.8 ± 3.6 hrs. for *sax-3(ky123)* vs. 42 hrs. for wild type; $P < 0.001$). These data indicate that *sax-3* mutants have metabolic or mitochondrial defects that are similar to *vpr-1* mutants, but most defects are less severe or occur with reduced frequency.

sax-3 Robo is expressed in motor neurons and body wall muscle (Chang et al., 2004; Kohara, 2001; Zallen et al., 1998). To test whether *sax-3* functions in muscle, we conducted two experiments. In the first, we expressed SAX-3 specifically in muscle of *sax-3(ky123)* mutants using the *myo-3* promoter. Muscle-specific SAX-3 expression strongly rescued the *sax-3(ky123)* muscle mitochondrial defects (Fig. 7A; rescue observed in 27/31 transgenic worms). Next, we specifically depleted SAX-3 in body wall muscle of wild-type worms using an RNAi mosaic strategy (Durieux et al., 2011; Esposito et al., 2007). *sid-1* mutants are defective for systemic RNAi, yet undergo cell autonomous RNAi normally (Winston et al., 2002). We specifically expressed *sax-3* sense and antisense RNAs (creating dsRNA) in *sid-1(pk3321)* muscle and examined their mitochondria. Muscle-specific *sax-3* RNAi caused mitochondrial defects nearly identical to those seen in *sax-3* mutants (Fig. 7A). These results indicate that *sax-3* functions cell autonomously in body wall muscle to influence mitochondria.

Our RNAi screen also identified the CLR-1 Lar receptor as a muscle mitochondrial regulator. In *clr-1* RNAi and *clr-1(e1745)ts* mutant adults, most mitochondria are positioned at the I-bands, but tubule length is much shorter than in the wild type (Fig. 6A and Table S1, lines 1 and 4). Despite the abnormal appearance of mitochondria, Mitotracker CMXRos staining did not show decreased transmembrane potential (Fig. 6B). *clr-1* is an essential gene required in hypodermal cells for fluid balance and the *e1745* allele is temperature sensitive (Huang and Stern, 2004; Kokel et al., 1998). We conducted temperature shift experiments to assess the temporal requirement of *clr-1* function. At the permissive temperature, *clr-1(e1745)ts* adult muscles contain mostly tubular mitochondria similar to the wild type. When young adults were shifted to the restrictive temperature for 12 hours, globular mitochondria were observed similar to *clr-1* RNAi animals (Fig. 6A). These results demonstrate that CLR-1 Lar is required in adults to maintain mitochondrial elongation on the I-bands. To test whether *clr-1* functions in muscle, we specifically depleted *clr-1* in body wall muscle using the *sid-1* mutant RNAi mosaic strategy. Muscle-specific CLR-1 depletion caused the same mitochondrial defects as those seen in *clr-1* RNAi and *clr-1(e1745)* mutants (Fig. 7A). In contrast, hypodermis-specific *clr-1* RNAi caused fluid accumulation, but not muscle mitochondrial defects (data not shown). Taken together, the data indicate that SAX-3 Robo and CLR-1 Lar function in muscle to influence mitochondria.

VPR-1 and SAX-3 Robo antagonize CLR-1 Lar signaling

Our data indicate that SAX-3 Robo and CLR-1 Lar function in muscle, yet their mutant phenotypes are clearly different (Fig. 6A). The *sax-3* mutant mitochondrial defects are nearly identical to the *vpr-1* mutant defects. To examine the signaling hierarchy between *vpr-1* and *sax-3*, we compared single and double null mutant strains. TEMs show that mitochondrial shape, including cross-sectional area, and positions in the double mutants are

identical to single null *vpr-1* mutants (Table S1, lines 2 and 5, $P > 0.1$; data not shown). In addition, ATP concentration in *vpr-1(tm1411); sax-3(ky123)* double mutants is not significantly different than *sax-3(ky123)* null mutants (Fig. 6D). Unfortunately, we were unable to generate mitoGFP transgenic lines in the double mutants. Taken together with the binding data, the results support the model that vMSPs positively regulate SAX-3 Robo.

Robo receptors antagonize Lar receptor signaling during *C. elegans* and *Drosophila* growth cone guidance decisions (Chang et al., 2004; Sun et al., 2000). Consistent with this relationship, the globular mitochondrial morphology in *clr-1* Lar mutants contrasts with the elongated morphology in VAP and Robo mutants (Figs. 1E and 6A). To examine the signaling hierarchy, we compared *vpr-1(tm1411); clr-1* RNAi mutants to *vpr-1(tm1441)* mutants using the mitoGFP marker. *clr-1* loss strongly suppresses the muscle mitochondrial defects of *vpr-1* mutants (Fig. 7A; Table S1, lines 6 and 2) and muscle mitochondria in *vpr-1(tm1411); clr-1* RNAi mutants are similar in morphology and distribution to mitochondria in wild-type hermaphrodites. Importantly, they are also positioned at muscle I-bands (Table S1, line 6). MitoTracker CMXRos staining and time-lapse imaging indicate that *clr-1* loss suppresses the mitochondrial transmembrane potential and mobility defects of *vpr-1* mutants (Fig. 7B and data not shown). Thus, muscle mitochondria in *vpr-1(tm1411); clr-1* RNAi animals are largely normal. This important result indicates that excess CLR-1 activity specifically causes the *vpr-1* mutant muscle mitochondrial defects. Hence, VPR-1 antagonizes Lar signaling in muscle. Moreover, a redundant mechanism must exist that positions mitochondria in the absence of VPR-1 and CLR-1.

The data support the model that SAX-3 Robo helps vMSPs antagonize CLR-1 Lar signaling. To further test this model, we generated *clr-1(e1745)ts; sax-3(ky123)* double mutants that express mitoGFP. The mitochondrial branching and elongation defects caused by *sax-3* loss are suppressed in the double mutant adults (Fig. 7A). Furthermore, mitochondria in the double mutants localize correctly to the I-bands. Therefore, VPR-1 and SAX-3 Robo antagonize CLR-1 Lar signaling in muscle to position mitochondria at I-bands. The simplest interpretation is that SAX-3 Robo facilitates vMSP binding to CLR-1 Lar or SAX-3/CLR-1 complexes.

VAP/Robo/Lar signaling modulates the Arp2/3 complex

Robo and Lar-like growth cone guidance receptors regulate the actin cytoskeleton, which can influence mitochondrial localization, either through direct interactions with F-actin or myosin motors (Boldogh and Pon, 2007; Pathak et al., 2010). To examine actin distribution in body wall muscle, we expressed the filamentous actin binding domain of moesin fused to GFP (Fig. 8A). In wild-type muscle, actin was observed in parallel arrays comprising the thin filaments, an I-band component. Little filamentous actin was observed in the muscle belly. While no difference in actin was observed in the sarcomeres of wild-type and *vpr-1* mutant muscle, the latter had extensive actin networks within the muscle belly (Fig. 8A). These ectopic actin networks occupy the same position as mitochondria, suggesting that their locations are mechanistically linked. Consistent with this idea, RNAi of genes encoding regulators of the actin cytoskeleton, including known downstream mediators of Robo and Lar receptor signaling, caused muscle mitochondrial defects (Fig. S5).

The Arp2/3 complex promotes actin nucleation and branching. Given the branched filament networks in *vpr-1* mutant muscle bellies, we hypothesized that aberrant Arp2/3 activity in the belly displaces mitochondria from I-bands, contributing to the mitochondrial defects. To test this hypothesis, we used RNAi to deplete Arp2/3 complex components in *vpr-1* mutants. *arx-2/arp2*, *arx-3/arp3*, or *arx-5/arp5* RNAi suppresses the mitochondrial morphology and distribution defects of *vpr-1* mutants (Fig. 8B). mitoGFP imaging and TEMs of *vpr-1(tm1411); arx-2* RNAi muscle indicate that large mitochondria correctly localize to I-

bands (Fig. 2D and Table S1, lines 2 and 7). Hence, aberrant Arp2/3 activity causes the VAP mutant mitochondrial defects. The Arp2/3 and CLR-1 Lar suppression data provide unequivocal evidence that these mitochondrial defects are specific and regulatory in nature. Finally, Arp2/3 inactivation in wild-type muscle causes mitochondrial morphology similar to those seen following Lar inactivation (Fig. 8B and Table S1, lines 8 and 4). These data support the model that vMSP/Robo/Lar signaling modulates Arp2/3 activity to position mitochondria at I-bands.

DISCUSSION

EphR, Robo, and Lar-like receptors are called growth cone guidance receptors because of their established roles in regulating the actin cytoskeleton during nervous system development. However, these receptors are also expressed after guidance decisions are made, particularly in the adult central nervous system and muscles (Longo et al., 1993; Zabolotny et al., 2001; Zhang and Goldstein, 1991). Here we show that Robo and Lar-like receptor pathways act in adults to modulate mitochondrial localization and morphology. Our results and those from previous studies support the following model (Fig. 8C). VAP MSP domains are cleaved in the neuron cytoplasm and secreted into the external environment. vMSP interactions with Robo and Lar receptors down-regulate Lar signaling to the Arp2/3 complex in muscle, stabilizing mitochondria at the I-bands. In VAP mutants, aberrant Lar and Arp2/3 activity causes ectopic actin filaments in the muscle belly that displace mitochondria from the I-bands, promote mitochondrial mobility, elongation, and branching, and inhibit energy metabolism. We propose that vMSPs restrict Arp2/3 activity to the I-bands, thereby influencing mitochondrial morphology and fission/fusion balance. This neuron-governed mechanism may regulate energy metabolism in response to environmental, nutritional, or developmental cues. Evidence for the model and implications for neurodegenerative diseases are discussed below.

We show that VAPs and sperm-derived MSPs comprise an evolutionarily conserved ligand class that promotes mitochondrial localization and morphology. VAP, Robo, and Lar homologs are present in sponges, animals without neurons and muscles, suggesting that their role in regulating mitochondria is ancestral to their growth cone guidance function (Srivastava et al., 2010). The mechanism by which vMSPs regulate mitochondria appears similar to the mechanism by which Slit repels migrating axons (Chang et al., 2004; Sun et al., 2000). During nervous system development, Slit binding to Robo down-regulates Lar receptor signaling that promotes migration. Therefore, Robo acts upstream of Lar. We show that Robo is required for vMSP signaling upstream of Lar. The simplest interpretation of our genetic and binding data is that Robo facilitates vMSP binding to Lar or Robo/Lar complexes, down-regulating Lar signaling. However, determining the extent to which high affinity vMSP interactions depend upon receptor complex formation will require further investigation. Given that EphR, Robo, and Lar receptors are broadly expressed throughout the nervous system, it is possible that vMSPs influence mitochondria in neurons. dVAP regulates the presynaptic microtubule cytoskeleton (Pennetta et al., 2002), which controls mitochondrial transport along axons (Hollenbeck and Saxton, 2005). Therefore, neurons may secrete factors like VAPB that regulate mitochondria in muscles and neurons.

The actin cytoskeleton regulates mitochondrial position in *C. elegans* muscle, cultured *Drosophila* and chick neurons, cultured mammalian cells, and yeast (Boldogh and Pon, 2007; Chada and Hollenbeck, 2004; Pathak et al., 2010; Quintero et al., 2009; Starr and Han, 2002). The worm ANC-1 protein is thought to couple actin to mitochondria and *anc-1* mutants have globular muscle mitochondrial morphology similar to *arx-2* RNAi animals (Starr and Han, 2002). We show that vMSPs promote mitochondrial docking at muscle I-bands, actin-enriched sites containing structures analogous to focal adhesions (Lecroisey et

al., 2007). CLR-1 Lar and Arp2/3 are required for maintenance or elongation of mitochondrial tubules along I-bands, a process that may facilitate (and/or require) fusion. In *vpr-1* mutants, mitochondria mislocalize to the muscle belly along with ectopic actin filaments and form thin elongated branches with increased mobility, increased fusion/fission balance, and reduced transmembrane potential. Lar or Arp2/3 inactivation suppresses these defects, revealing an unexpected role for the actin cytoskeleton in modulating multiple aspects of mitochondrial biology. Whether Arp2/3 regulates mitochondria directly or indirectly through positioning or docking effects is not clear. The actin cytoskeleton has been shown to influence mitochondrial fission in cultured cells (De Vos et al., 2005; Pathak et al., 2010). vMSP signals are likely regulatory in nature, as a parallel mechanism promotes mitochondrial positioning in the absence of VAP and Arp2/3 function.

Defects in skeletal muscle mitochondria have been implicated in the pathology of ALS (Dupuis et al., 2004; Zhou et al., 2010). In mutant *sod1* transgenic mice, the SOD1 protein aberrantly accumulates in mitochondria (Wong et al., 1995; Kong and Xu, 1998) and causes skeletal muscle mitochondrial dysfunction that is initiated at the neuromuscular junction (Zhou et al., 2010). Subsarcolemmal aggregates of abnormal mitochondria with low transmembrane potential are found in skeletal muscle of these mice well before the onset of the disease (Zhou et al., 2010). ALS patients with a SOD1 mutation also show a muscle mitochondrial oxidative defect (Corti et al., 2009) and sporadic ALS patients have been documented with muscle mitochondrial respiratory chain dysfunction (Crugnola et al., 2010). Defects in muscle mitochondria may therefore, contribute as a primary cause in ALS pathogenesis. Indeed, uncoupling electron transport from ATP synthesis in muscle mitochondria by overexpressing uncoupling protein 1 is sufficient to initiate motor neuron degeneration (Dupuis et al., 2009).

Our results support the hypothesis that secreted vMSPs modulate mitochondrial position through growth cone guidance receptor pathways. It seems likely that this signaling mechanism plays a role in ALS pathogenesis. The $VAPB^{P56S}$ mutation inhibits wild-type and mutant MSP domain secretion (Tsuda et al., 2008). Reducing vMSP secretion might cause abnormal mitochondrial localization, morphology, and function in ALS8 patients. Consistent with this model, low VAP levels in sporadic ALS patients and mouse *sod1* models correlate with widespread mitochondrial abnormalities (Anagnostou et al., 2010; Dupuis et al., 2008; Dupuis et al., 2004; Teuling et al., 2007; Wong et al., 1995b). Moreover, analyses of data from whole-genome associated studies have discovered that single nucleotide polymorphisms within genes mediating growth cone guidance, including Robo, Lar, and Cdc42 are associated with susceptibility, survival, or onset of ALS (Lesnick et al., 2008). In addition, the discovery that growth cone guidance pathways influence mitochondria may have implications for other neurodegenerative diseases, such as spinal muscular atrophy and Parkinson's disease (Lesnick et al., 2007).

EXPERIMENTAL PROCEDURES

Genetics, RNAi, and plasmids

Bristol N2 is the wild-type *C. elegans* strain. Worms were maintained on NGM plates with NA22 bacteria at 20°C except where indicated otherwise. Strain construction and marker scoring were performed as previously described using PCR and phenotypic analyses (Miller et al., 2003; Tsuda et al., 2008). The *fog-2(q71)* mutation was used to generate male/female strains. RNAi was performed by the feeding method using HT115 bacterial strains (Kamath et al., 2003). Positive clones were sequenced for confirmation. See the Supplemental Experimental Procedures for additional information.

Staining, microinjection, and microscopy

Mitochondria were labeled using Mitotracker CMXRos, Rhodamine 6g, and mito::GFP, which targets the matrix. For Mitotracker CMXRos and Rhodamine 6g staining, dyes were added to seeded NGM plates (Labrousse et al., 1999). Imaging was done without anesthetics on dried 2% agarose pads immediately after mounting. Anesthetics can cause mitochondrial fragmentation. Images were taken using a motorized Zeiss Axioskop 2 with MRM Axiocam Hi-Res digital camera and Perkin Elmer Spinning Disc Nikon TE2000 microscope equipped with an EMCCD C9100-50 camera operated by Velocity 5.3 software. Purified recombinant MSP domains were microinjected into the gonad using a Zeiss Axiovert 200 microscope. Injected animals were mounted for direct observation after a 15 min. to 1 hr. recovery period.

Transgenics

To generate transgenic *C. elegans*, plasmids (60ng/μl) were mixed with pRF4 [*rol-6*] (60ng/μl), *myo-3p::mito::GFP* (60ng/μl), or *myo-2p::mCherry* (60ng/μl) and injected into young adult hermaphrodite gonads. The *myo-3p::mito::GFP* plasmid was generously provided by Dr. van der Bliek. Transgenic lines were selected based on the roller phenotype or GFP expression. Multiple independent transgenic lines were analyzed. Two *vpr-1(tm1411)/hT2; unc-119p::vpr-1* transgenic lines were integrated by gamma irradiation.

Fluorescence loss in photobleaching (FLIP)

FLIP was achieved with a Perkin Elmer Spinning Disc Nikon TE2000 microscope programmed to cycle between bleaching and scanning every 5 seconds for 4 minutes. The fluorescence intensities of indicated areas were analyzed in Volocity software (Perkin Elmer, UK). Animals were immobilized on dried 2% agarose pads under conditions that prevent animal and mitochondrial mobility (i.e. 1–3 animals per pad). Only muscles with immobile mitochondria were analyzed.

MSP binding assays

MSP-FITC and vMSP-FITC binding assays were conducted as previously described (Miller et al., 2003; Tsuda et al., 2008). Briefly, HEK293T cells were cultured on coverslips in 6-well plates and cells (~50% confluence) were transiently transfected with 2 μg of VAB-1, 3xFLAG::SAX-3, CLR-1::V5, or pcDNA3.2 control plasmids (Miller et al., 2003) using FuGENE HD transfection reagent, according to the manufacturer's instructions (Promega, U.S.A). The 3xFLAG::SAX-3 construct was generously provided by Dr. Joe Culotti. The CLR-1::V5 construct contained the CLR-1 extracellular and transmembrane domains, but not the phosphatase domains. After 24 hours, cells were incubated with MSP-FITC or vMSP-FITC for 30 minutes at 23°C and washed three times in 50 ml PBS. Transfected cells were preincubated with a 25-fold molar excess of unlabelled MSP to evaluate specific binding. Fluorescence was measured from linear range exposures using Axiovision software.

Metabolic assays

Resistance to paraquat (Ultra Scientific, U.S.A), ATP concentration measurement, oxygen consumption, and MitoTracker CMXRos staining methods are described in Supplemental Experimental Procedures. Oxygen consumption was measured at constant temperature (20°C) using the oxygraph system (Hansatech, UK).

Transmission electron microscopy

TEM was performed as previously described (Tsuda et al., 2008; Whitten and Miller, 2007). Care was taken to ensure that fixation occurred rapidly and cross sections were orthogonal

to muscle myofilaments. Mitochondria do not consistently localize to I-bands near neuromuscular junctions.

Supplementary Material

Refer to Web version on PubMed Central for supplementary material.

Acknowledgments

We thank the *Caenorhabditis* Genetics Center (funded by the NIH Center for Research Resources) for strains, J. Culotti, D. Sherwood, and A. van der Bliek for plasmids, G. Marques and the Yoder lab for help with confocal miscroscopy, and Tim Mahoney, Manish Jaiswal, Hector Sandoval, Vafa Bayat, Chao Tong, and Jennifer Zallen for comments on the manuscript. This work was supported in part by the American Cancer Society (RSG-06-151-01-DDC to M.A.M.), Muscular Dystrophy Association (MDA186119 to M.A.M) and a UAB Clinical Nutrition Center Nutrition or Obesity-Related Pilot Feasibility Studies grant (UAB NORC grant P30DK056336). H.J.B. is an Investigator of the HHMI.

REFERENCES

Anagnostou G, Akbar MT, Paul P, Angelinetta C, Steiner TJ, de Belleroche J. Vesicle associated membrane protein B (VAPB) is decreased in ALS spinal cord. Neurobiol Aging. 2010; 31:969–985. [PubMed: 18701194]

Boldogh IR, Pon LA. Mitochondria on the move. Trends Cell Biol. 2007; 17:502–510. [PubMed: 17804238]

Bottino D, Mogilner A, Roberts T, Stewart M, Oster G. How nematode sperm crawl. J Cell Sci. 2002; 115:367–384. [PubMed: 11839788]

Chada SR, Hollenbeck PJ. Nerve growth factor signaling regulates motility and docking of axonal mitochondria. Curr Biol. 2004; 14:1272–1276. [PubMed: 15268858]

Chai A, Withers J, Koh YH, Parry K, Bao H, Zhang B, Budnik V, Pennetta G. hVAPB, the causative gene of a heterogeneous group of motor neuron diseases in humans, is functionally interchangeable with its Drosophila homologue DVAP-33A at the neuromuscular junction. Hum Mol Genet. 2008; 17:266–280. [PubMed: 17947296]

Chang C, Yu TW, Bargmann CI, Tessier-Lavigne M. Inhibition of netrin-mediated axon attraction by a receptor protein tyrosine phosphatase. Science. 2004; 305:103–106. [PubMed: 15232111]

Corti S, Donadoni C, Ronchi D, Bordoni A, Fortunato F, Santoro D, Del Bo R, Lucchini V, Crugnola V, Papadimitriou D, et al. Amyotrophic lateral sclerosis linked to a novel SOD1 mutation with muscle mitochondrial dysfunction. J Neurol Sci. 2009; 276:170–174. [PubMed: 19000626]

Crugnola V, Lamperti C, Lucchini V, Ronchi D, Peverelli L, Prelle A, Sciacco M, Bordoni A, Fassone E, Fortunato F, et al. Mitochondrial respiratory chain dysfunction in muscle from patients with amyotrophic lateral sclerosis. Arch Neurol. 2010; 67:849–854. [PubMed: 20625092]

De Vos KJ, Allan VJ, Grierson AJ, Sheetz MP. Mitochondrial function and actin regulate dynamin-related protein 1-dependent mitochondrial fission. Curr Biol. 2005; 15:678–683. [PubMed: 15823542]

Dupuis L, Corcia P, Fergani A, Gonzalez De Aguilar JL, Bonnefont-Rousselot D, Bittar R, Seilhean D, Hauw JJ, Lacomblez L, Loeffler JP, et al. Dyslipidemia is a protective factor in amyotrophic lateral sclerosis. Neurology. 2008; 70:1004–1009. [PubMed: 18199832]

Dupuis L, Gonzalez de Aguilar JL, Echaniz-Laguna A, Eschbach J, Rene F, Oudart H, Halter B, Huze C, Schaeffer L, Bouillaud F, et al. Muscle mitochondrial uncoupling dismantles neuromuscular junction and triggers distal degeneration of motor neurons. PLoS One. 2009; 4:e5390. [PubMed: 19404401]

Dupuis L, Gonzalez de Aguilar JL, Oudart H, de Tapia M, Barbeito L, Loeffler JP. Mitochondria in amyotrophic lateral sclerosis: a trigger and a target. Neurodegener Dis. 2004; 1:245–254. [PubMed: 16908975]

Durieux J, Wolff S, Dillin A. The Cell-Non-Autonomous Nature of Electron Transport Chain-Mediated Longevity. Cell. 2011; 144:79–91. [PubMed: 21215371]

Esposito G, Di Schiavi E, Bergamasco C, Bazzicalupo P. Efficient and cell specific knock-down of gene function in targeted C-elegans neurons. Gene. 2007; 395:170–176. [PubMed: 17459615]

Fares H, Greenwald I. Genetic analysis of endocytosis in Caenorhabditis elegans: Coelomocyte uptake defective mutants. Genetics. 2001; 159:133–145. [PubMed: 11560892]

Funke AD, Esser M, Kruttgen A, Weis J, Mitne-Neto M, Lazar M, Nishimura AL, Sperfeld AD, Trillenberg P, Senderek J, et al. The p.P56S mutation in the VAPB gene is not due to a single founder: the first European case. Clin Genet. 2010; 77:302–303. [PubMed: 20447143]

Gkogkas C, Wardrope C, Hannah M, Skehel P. The ALS8-associated mutant VAPBP56S is resistant to proteolysis in neurons. Journal of Neurochemistry. 2011; 117:286–294. [PubMed: 21275991]

Govindan JA, Nadarajan S, Kim S, Starich TA, Greenstein D. Somatic cAMP signaling regulates MSP-dependent oocyte growth and meiotic maturation in C. elegans. Development. 2009; 136:2211–2221. [PubMed: 19502483]

Han SM, Cottee PA, Miller MA. Sperm and oocyte communication mechanisms controlling C. elegans fertility. Dev Dyn. 2010; 239:1265–1281. [PubMed: 20034089]

Hao JC, Yu TW, Fujisawa K, Culotti JG, Gengyo-Ando K, Mitani S, Moulder G, Barstead R, Tessier-Lavigne M, Bargmann CI. C. elegans slit acts in midline, dorsal-ventral, and anterior-posterior guidance via the SAX-3/Robo receptor. Neuron. 2001; 32:25–38. [PubMed: 11604136]

Hollenbeck PJ, Saxton WM. The axonal transport of mitochondria. J Cell Sci. 2005; 118:5411–5419. [PubMed: 16306220]

Huang P, Stern MJ. FGF signaling functions in the hypodermis to regulate fluid balance in C. elegans. Development. 2004; 131:2595–2604. [PubMed: 15115754]

Kamath RS, Fraser AG, Dong Y, Poulin G, Durbin R, Gotta M, Kanapin A, Le Bot N, Moreno S, Sohrmann M, et al. Systematic functional analysis of the Caenorhabditis elegans genome using RNAi. Nature. 2003; 421:231–237. [PubMed: 12529635]

Kanazawa T, Zappaterra MD, Hasegawa A, Wright AP, Newman-Smith ED, Buttle KF, McDonald K, Mannella CA, van der Bliek AM. The C. elegans Opa1 homologue EAT-3 is essential for resistance to free radicals. PLoS Genet. 2008; 4:e1000022. [PubMed: 18454199]

Kohara Y. Systematic analysis of gene expression of the C. elegans genome. Tanpakushitsu Kakusan Koso. 2001; 46:2425–2431. [PubMed: 11802405]

Kokel M, Borland CZ, DeLong L, Horvitz HR, Stern MJ. clr-1 encodes a receptor tyrosine phosphatase that negatively regulates an FGF receptor signaling pathway in Caenorhabditis elegans. Genes Dev. 1998; 12:1425–1437. [PubMed: 9585503]

Labrousse AM, Zappaterra MD, Rube DA, van der Bliek AM. C. elegans dynamin-related protein DRP-1 controls severing of the mitochondrial outer membrane. Mol Cell. 1999; 4:815–826. [PubMed: 10619028]

Lecroisey C, Segalat L, Gieseler K. The C. elegans dense body: anchoring and signaling structure of the muscle. J Muscle Res Cell Motil. 2007; 28:79–87. [PubMed: 17492481]

Lesnick TG, Papapetropoulos S, Mash DC, Ffrench-Mullen J, Shehadeh L, de Andrade M, Henley JR, Rocca WA, Ahlskog JE, Maraganore DM. A genomic pathway approach to a complex disease: axon guidance and Parkinson disease. PLoS Genet. 2007; 3:e98. [PubMed: 17571925]

Lesnick TG, Sorenson EJ, Ahlskog JE, Henley JR, Shehadeh L, Papapetropoulos S, Maraganore DM. Beyond Parkinson disease: amyotrophic lateral sclerosis and the axon guidance pathway. PLoS One. 2008; 3:e1449. [PubMed: 18197259]

Lev S, Ben Halevy D, Peretti D, Dahan N. The VAP protein family: from cellular functions to motor neuron disease. Trends Cell Biol. 2008; 18:282–290. [PubMed: 18468439]

Longo FM, Martignetti JA, Le Beau JM, Zhang JS, Barnes JP, Brosius J. Leukocyte common antigen-related receptor-linked tyrosine phosphatase. Regulation of mRNA expression. J Biol Chem. 1993; 268:26503–26511. [PubMed: 8253779]

Millecamps S, Salachas F, Cazeneuve C, Gordon P, Bricka B, Camuzat A, Guillot-Noel L, Russaouen O, Bruneteau G, Pradat PF, et al. SOD1, ANG, VAPB, TARDBP, and FUS mutations in familial amyotrophic lateral sclerosis: genotype-phenotype correlations. J Med Genet. 2010

Miller MA, Nguyen VQ, Lee MH, Kosinski M, Schedl T, Caprioli RM, Greenstein D. A sperm cytoskeletal protein that signals oocyte meiotic maturation and ovulation. Science. 2001; 291:2144–2147. [PubMed: 11251118]

Miller MA, Ruest PJ, Kosinski M, Hanks SK, Greenstein D. An Eph receptor sperm-sensing control mechanism for oocyte meiotic maturation in Caenorhabditis elegans. Genes Dev. 2003; 17:187–200. [PubMed: 12533508]

Mitne-Neto M, Machado-Costa M, Marchetto MC, Bengtson MH, Joazeiro CA, Tsuda H, Bellen HJ, Silva HC, Oliveira AS, Lazar M, et al. Downregulation of VAPB expression in motor neurons derived from induced pluripotent stem cells of ALS8 patients. Hum Mol Genet. 2011; 20:3642–3652. [PubMed: 21685205]

Nishimura AL, Mitne-Neto M, Silva HC, Richieri-Costa A, Middleton S, Cascio D, Kok F, Oliveira JR, Gillingwater T, Webb J, et al. A mutation in the vesicle-trafficking protein VAPB causes late-onset spinal muscular atrophy and amyotrophic lateral sclerosis. Am J Hum Genet. 2004; 75:822–831. [PubMed: 15372378]

Parekh AB. Mitochondrial regulation of intracellular Ca2+ signaling: more than just simple Ca2+ buffers. News Physiol Sci. 2003; 18:252–256. [PubMed: 14614159]

Pathak D, Sepp KJ, Hollenbeck PJ. Evidence that myosin activity opposes microtubule-based axonal transport of mitochondria. J Neurosci. 2010; 30:8984–8992. [PubMed: 20592219]

Pennetta G, Hiesinger P, Fabian-Fine R, Meinertzhagen I, Bellen H. Drosophila VAP-33A directs bouton formation at neuromuscular junctions in a dosage-dependent manner. Neuron. 2002; 35:291–306. [PubMed: 12160747]

Quintero OA, DiVito MM, Adikes RC, Kortan MB, Case LB, Lier AJ, Panaretos NS, Slater SQ, Rengarajan M, Feliu M, et al. Human Myo19 is a novel myosin that associates with mitochondria. Curr Biol. 2009; 19:2008–2013. [PubMed: 19932026]

Ratnaparkhi A, Lawless GM, Schweizer FE, Golshani P, Jackson GR. A Drosophila model of ALS: human ALS-associated mutation in VAP33A suggests a dominant negative mechanism. PLoS ONE. 2008; 3:e2334. [PubMed: 18523548]

Reinke V, Gil IS, Ward S, Kazmer K. Genome-wide germline-enriched and sex-biased expression profiles in Caenorhabditis elegans. Development. 2004; 131:311–323. [PubMed: 14668411]

Srivastava M, Simakov O, Chapman J, Fahey B, Gauthier ME, Mitros T, Richards GS, Conaco C, Dacre M, Hellsten U, et al. The Amphimedon queenslandica genome and the evolution of animal complexity. Nature. 2010; 466:720–726. [PubMed: 20686567]

Starr DA, Han M. Role of ANC-1 in tethering nuclei to the actin cytoskeleton. Science. 2002; 298:406–409. [PubMed: 12169658]

Suen DF, Norris KL, Youle RJ. Mitochondrial dynamics and apoptosis. Genes Dev. 2008; 22:1577–1590. [PubMed: 18559474]

Sun Q, Bahri S, Schmid A, Chia W, Zinn K. Receptor tyrosine phosphatases regulate axon guidance across the midline of the Drosophila embryo. Development. 2000; 127:801–812. [PubMed: 10648238]

Teuling E, Ahmed S, Haasdijk E, Demmers J, Steinmetz MO, Akhmanova A, Jaarsma D, Hoogenraad CC. Motor neuron disease-associated mutant vesicle-associated membrane protein-associated protein (VAP) B recruits wild-type VAPs into endoplasmic reticulum-derived tubular aggregates. J Neurosci. 2007; 27:9801–9815. [PubMed: 17804640]

Tsang WY, Lemire BD. The role of mitochondria in the life of the nematode, Caenorhabditis elegans. Biochim Biophys Acta. 2003; 1638:91–105. [PubMed: 12853115]

Tsuda H, Han SM, Yang Y, Tong C, Lin YQ, Mohan K, Haueter C, Zoghbi A, Harati Y, Kwan J, et al. The amyotrophic lateral sclerosis 8 protein VAPB is cleaved, secreted, and acts as a ligand for Eph receptors. Cell. 2008; 133:963–977. [PubMed: 18555774]

Vendelin M, Beraud N, Guerrero K, Andrienko T, Kuznetsov AV, Olivares J, Kay L, Saks VA. Mitochondrial regular arrangement in muscle cells: a "crystal-like" pattern. Am J Physiol Cell Physiol. 2005; 288:C757–C767. [PubMed: 15496480]

Whitten SJ, Miller MA. The role of gap junctions in Caenorhabditis elegans oocyte maturation and fertilization. Dev Biol. 2007; 301:432–446. [PubMed: 16982048]

Winston WM, Molodowitch C, Hunter CP. Systemic RNAi in C. elegans requires the putative transmembrane protein SID-1. Science. 2002; 295:2456–2459. [PubMed: 11834782]

Wolke U, Jezuit EA, Priess JR. Actin-dependent cytoplasmic streaming in C. elegans oogenesis. Development. 2007; 134:2227–2236. [PubMed: 17507392]

Wong A, Boutis P, Hekimi S. Mutations in the clk-1 gene of Caenorhabditis elegans affect developmental and behavioral timing. Genetics. 1995a; 139:1247–1259. [PubMed: 7768437]

Wong PC, Pardo CA, Borchelt DR, Lee MK, Copeland NG, Jenkins NA, Sisodia SS, Cleveland DW, Price DL. An adverse property of a familial ALS-linked SOD1 mutation causes motor neuron disease characterized by vacuolar degeneration of mitochondria. Neuron. 1995b; 14:1105–1116. [PubMed: 7605627]

Yang Y, Han SM, Miller MA. MSP hormonal control of the oocyte MAP kinase cascade and reactive oxygen species signaling. Dev Biol. 2010; 342:96–107. [PubMed: 20380830]

Zabolotny JM, Kim YB, Peroni OD, Kim JK, Pani MA, Boss O, Klaman LD, Kamatkar S, Shulman GI, Kahn BB, et al. Overexpression of the LAR (leukocyte antigen-related) protein-tyrosine phosphatase in muscle causes insulin resistance. Proc Natl Acad Sci U S A. 2001; 98:5187–5192. [PubMed: 11309481]

Zallen JA, Yi BA, Bargmann CI. The conserved immunoglobulin superfamily member SAX-3/Robo directs multiple aspects of axon guidance in C. elegans. Cell. 1998; 92:217–227. [PubMed: 9458046]

Zhang WR, Goldstein BJ. Identification of skeletal muscle protein-tyrosine phosphatases by amplification of conserved cDNA sequences. Biochem Biophys Res Commun. 1991; 178:1291–1297. [PubMed: 1651716]

Zhou J, Yi J, Fu R, Liu E, Siddique T, Rios E, Deng HX. Hyperactive intracellular calcium signaling associated with localized mitochondrial defects in skeletal muscle of an animal model of amyotrophic lateral sclerosis. J Biol Chem. 2010; 285:705–712. [PubMed: 19889637]

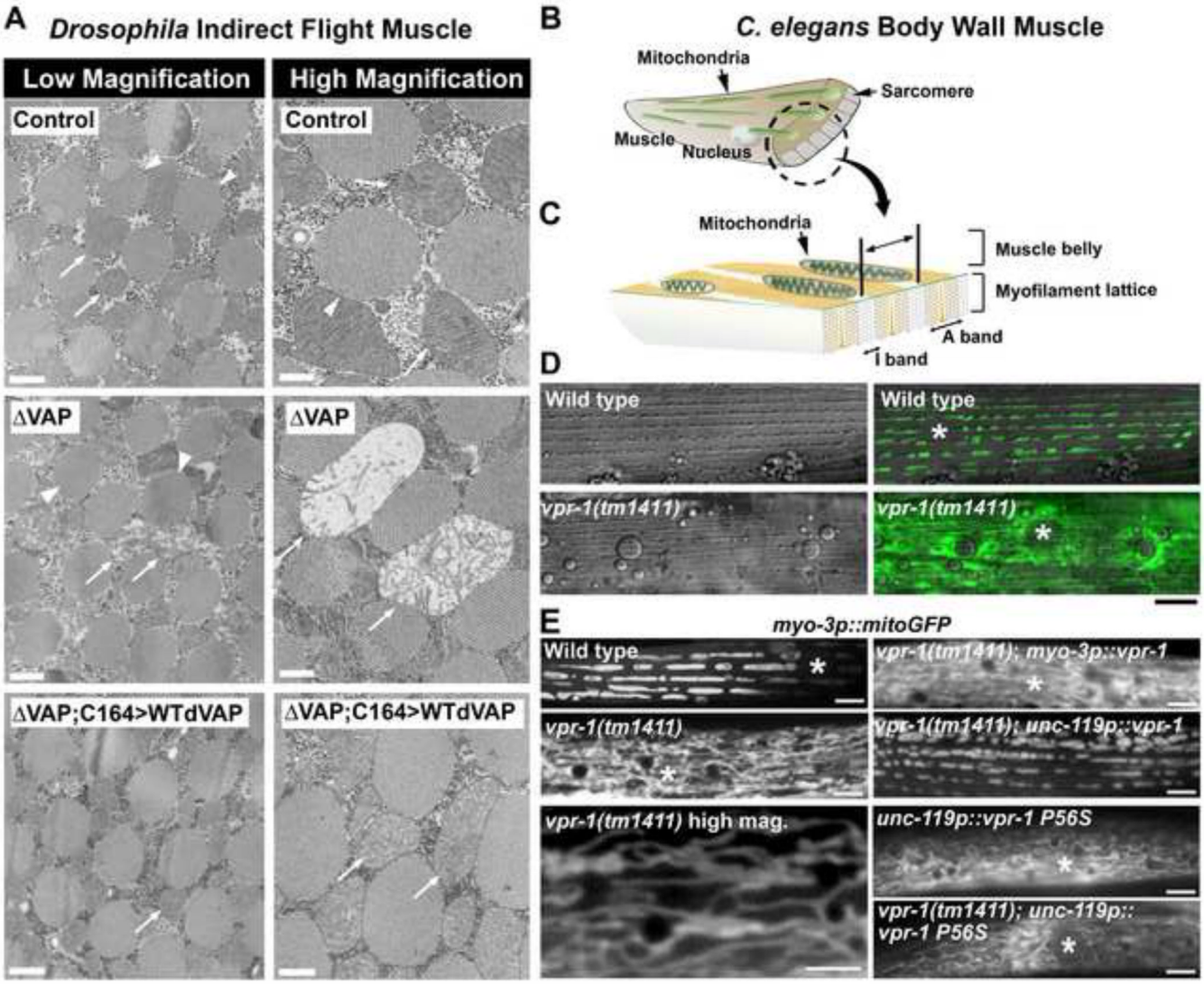

Figure 1. Neuronal VAPs modulate striated muscle mitochondrial morphology in *Drosophila* and *C. elegans*

(A) Transmission electron micrographs of adult IFM (dorsal ventral) in wild-type control and mutant flies. Arrowheads indicate myofibrils and arrows indicate mitochondria. ΔVAP indicates *dvap* null mutant and C164>WTdVAP indicates wild-type dVAP expression using the neuronal GAL4 driver, C164 GAL4. Low mag. bars, 1.0 μm; high mag. bars, 0.5 μm.

(B and C) *C. elegans* body wall muscle cell diagrams showing mitochondrial arrays (B) and basic myofilament structure (C).

(D) Muscle mitochondria tubules visualized using mitochondrial matrix-targeted GFP (mitoGFP) and dense bodies (small bumps running in parallel) visualized using DIC imaging. Dense bodies occupy the center of the I-band. Quantification is shown in Table S1. Asterisks indicate nucleus. Bar, 5 μm.

(E) Mitochondrial networks in wild-type and mutant body wall muscle. Neuronal expression is driven with the *unc-119* promoter and muscle expression is driven with the *myo-3* promoter. Asterisks indicate nucleus. Bars, 5 μm.

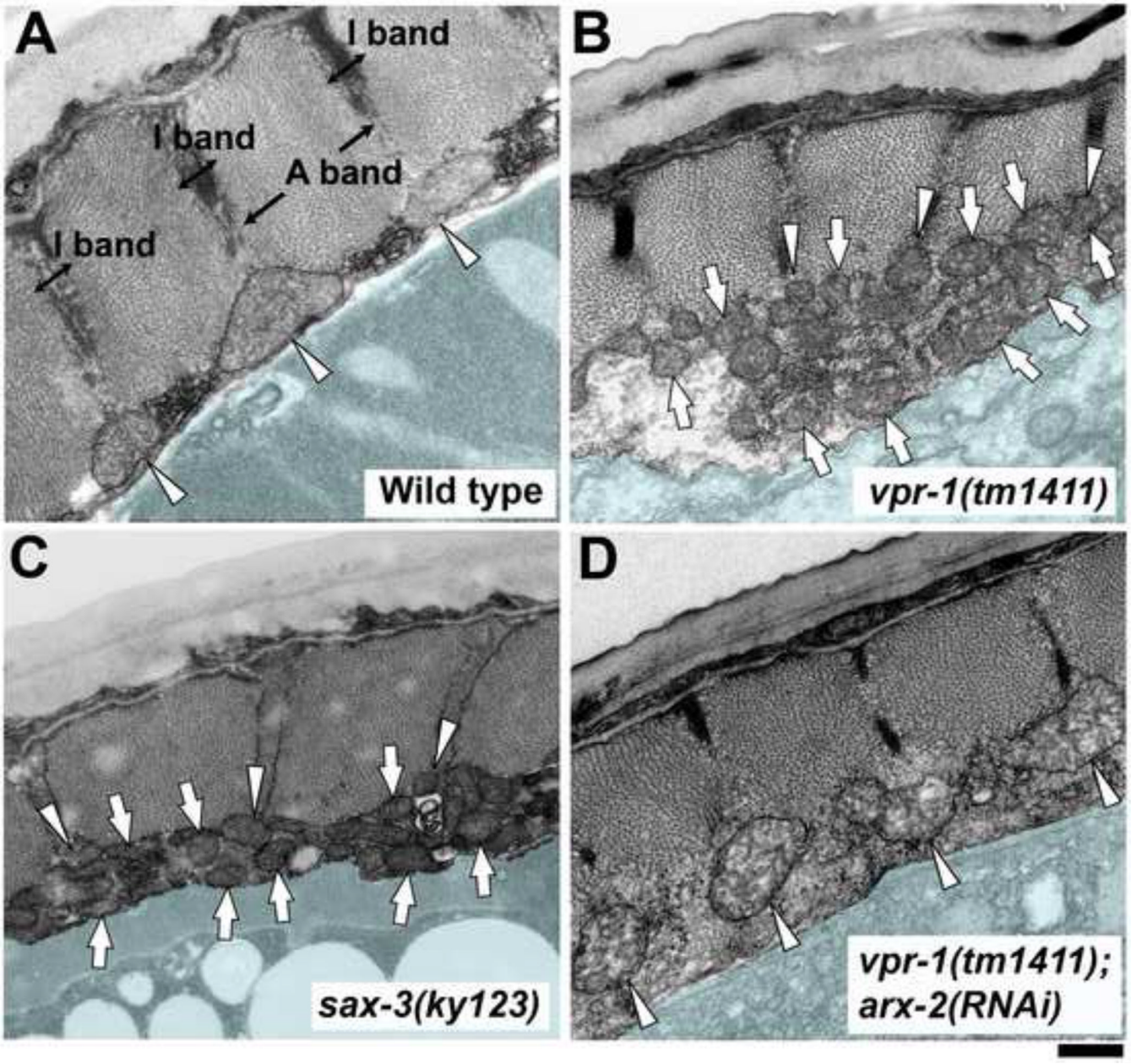

Figure 2. Transmission electron micrographs of wild-type and mutant *C. elegans* muscle

(A–D) Adult body wall muscle cross sections are shown. Arrowheads point to mitochondria with I-band localization, whereas arrows point to mitochondria with abnormal localization. Light blue color demarcates muscle boundary. Bar, 0.5 μm.

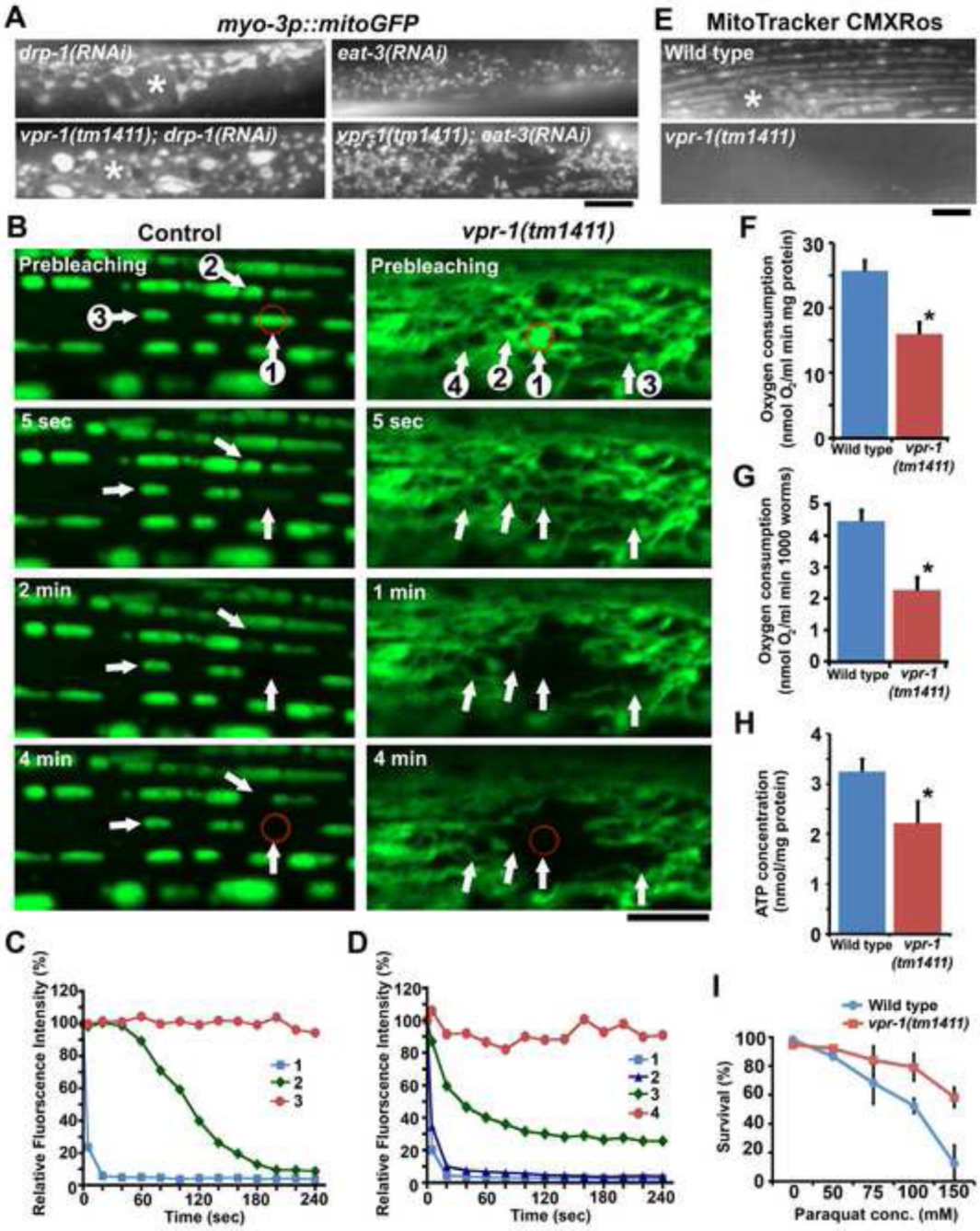

Figure 3. *vpr-1* loss influences muscle mitochondrial connectivity and function

(A) Genetic relationships between *vpr-1* and the mitochondrial fission mediator *drp-1* or the fusion mediator *eat-3*. Asterisks indicate nucleus. Bar, 5 μm.

(B) MitoGFP fluorescence loss in photobleaching of wild-type control and *vpr-1* mutant muscle. The red circle indicates the area of laser bleaching. Fluorescence was measured throughout the field after each 5 second cycle. Intensities of numbered spots are shown in panels C and D. Bar, 5 μm.

(C and D) Quantification of fluorescence intensities in indicated mitochondria (panel B) of control (C) and *vpr-1* mutant (D) muscles.

(E) MitoTracker CMXRos staining of wild-type and *vpr-1(tm1411)* mutant muscle. Bar, 5 μm.

(F and G) Oxygen consumption rates of wild-type and mutant hermaphrodites. Consumption rates were normalized by protein content (F) or number of worms (G). *, $P < 0.001$. Error bars represent SD.

(H) ATP concentration in wild-type and mutant hermaphrodite extracts. *, $P < 0.001$ compared to wild type. Error bars represent SD.

(I) Paraquat sensitivity in wild-type and *vpr-1(tm1411)* hermaphrodites. Error bars represent SD.

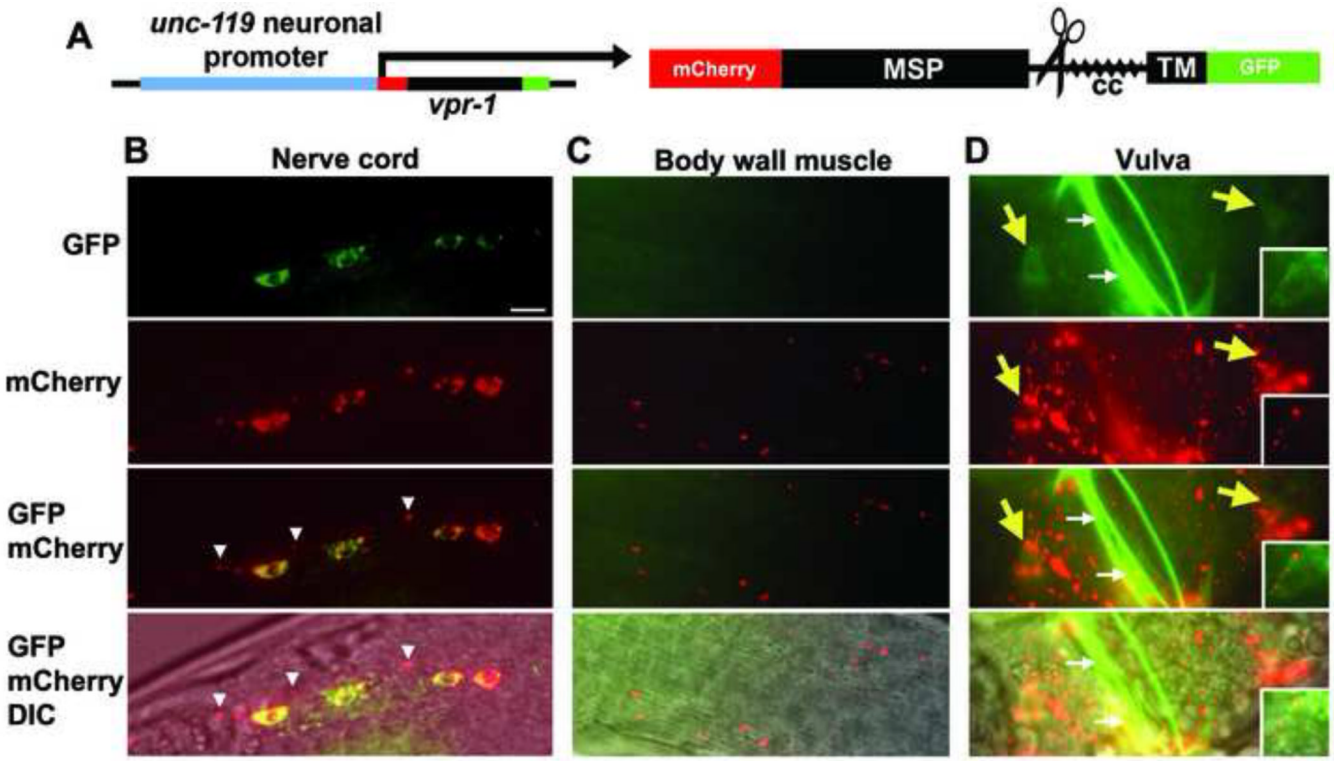

Figure 4. VAP cleavage and secretion in *C. elegans* neurons

(A) Diagrams of the mCherry::VPR-1::GFP fusion protein driven specifically in neurons. Scissors show region of cleavage. cc, coiled coil domain.

(B) Fusion protein expression in nerve cord motor neurons. Arrowheads indicate examples of mCherry/MSP-containing complexes that lack GFP-containing sequences. Bar, 5 μm.

(C) Fusion protein localization outside of neuronal cell bodies.

(D) Fusion protein localization in the vulva region. VC4 and VC5 motor neuron cell bodies (yellow arrows) are in the background (behind the focal plane). Inset shows the HSN motor neuron cell body. Longer mCherry exposure times show mCherry co-localization with GFP in the cytoplasm. The vulva lip exhibits nonspecific autofluorescence seen in nontransgenic controls (white arrows). The *rol-6* transgenic marker may cause mCherry/MSP aggregates, as more uniform extracellular mCherry/MSP distribution is seen with other transgenic markers.

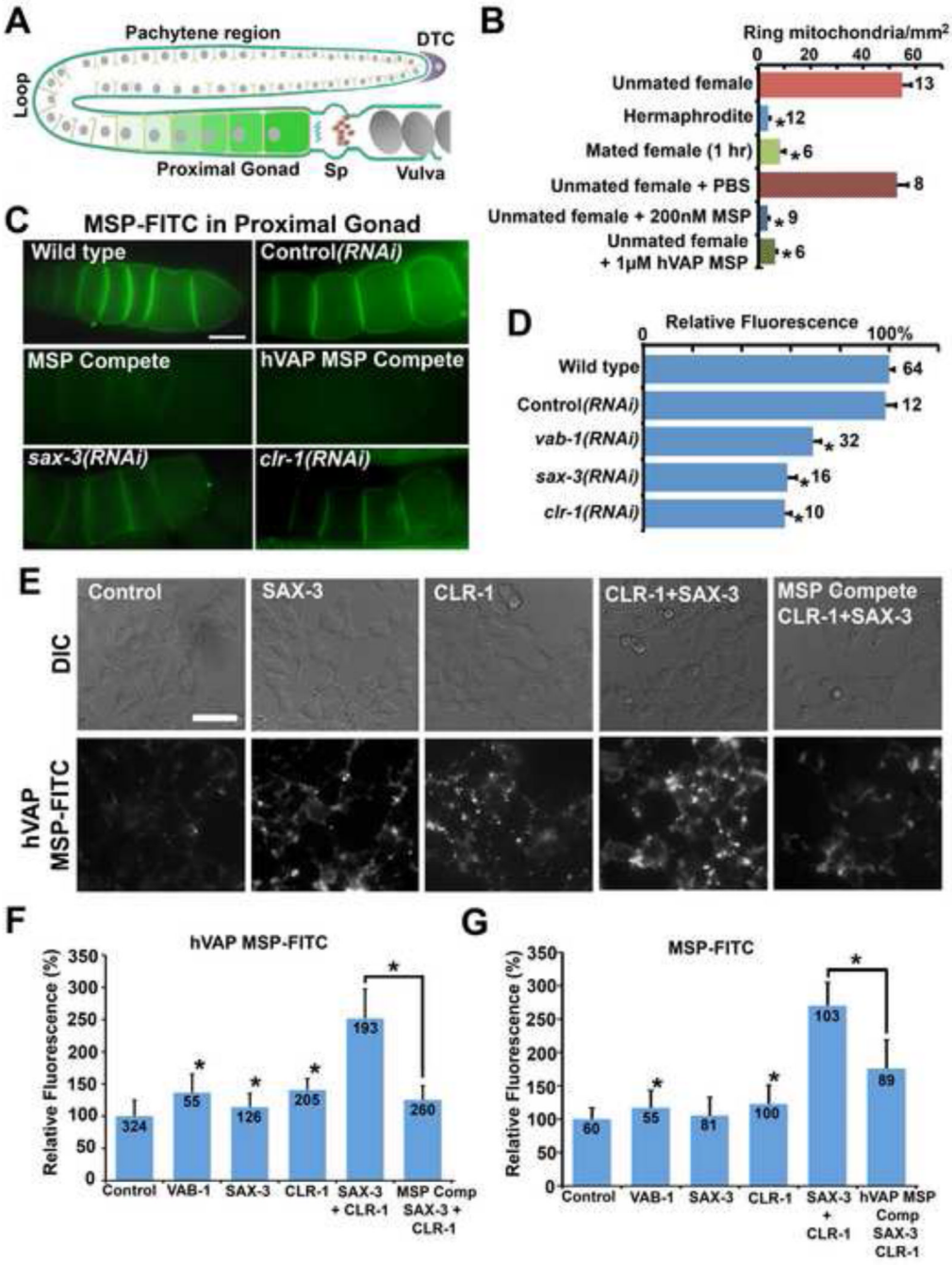

Figure 5. An MSP receptor screen identifies SAX-3 Robo and CLR-1 Lar-like receptors

(A) Diagram of the *C. elegans* adult gonad. Mitochondrial morphology and MSP domain binding were quantified in oocytes colored green (panels B–D and Fig. S4). DTC, distal tip cell; Sp, spermatheca.

(B) Quantification of ring-shaped mitochondria per mm^2 oocyte area in the presence and absence of extracellular MSP domains introduced by mating and microinjection. MSP domains were injected through the vulva into the reproductive tract of unmated females lacking sperm. See Fig. S4A–D for representative pictures of oocyte mitochondria. *, $P < 0.001$ compared to unmated female controls. Error bars represent SEM.

(C) 200 nM MSP-FITC binding to oocyte plasma membranes. In the compete panels, a 20-fold molar excess of unlabelled MSP or hVAP MSP was added before the assay. Quantitative data is shown in panel D. Proximal is to the right, as shown in panel A (green). Bar, 20 μm.

(D) Quantitative MSP-FITC binding data for control and selected RNAi clones (N is to the right of error bars). *, $P < 0.001$ compared to wild type. Error bars represent SEM.

(E) 200 nM human VAP MSP-FITC was incubated with control transfected and receptor transfected HEK293T cells for 30 min, washed 3 times, and mounted for microscopy. vMSP-FITC was found at the cell surface and in intracellular vesicles of live cells. In the compete panel, a 20-fold molar excess of unlabelled MSP was added before the assay. Bar, 50 μm.

(F) Quantification of human VAP MSP-FITC fluorescence. *, $P < 0.001$ compared to control. Number of cells measured is shown below error bars, which represent SD.

(G) Quantification of MSP-FITC fluorescence. *, $P < 0.001$ compared to control. Number of cells measured is shown below error bars, which represent SD.

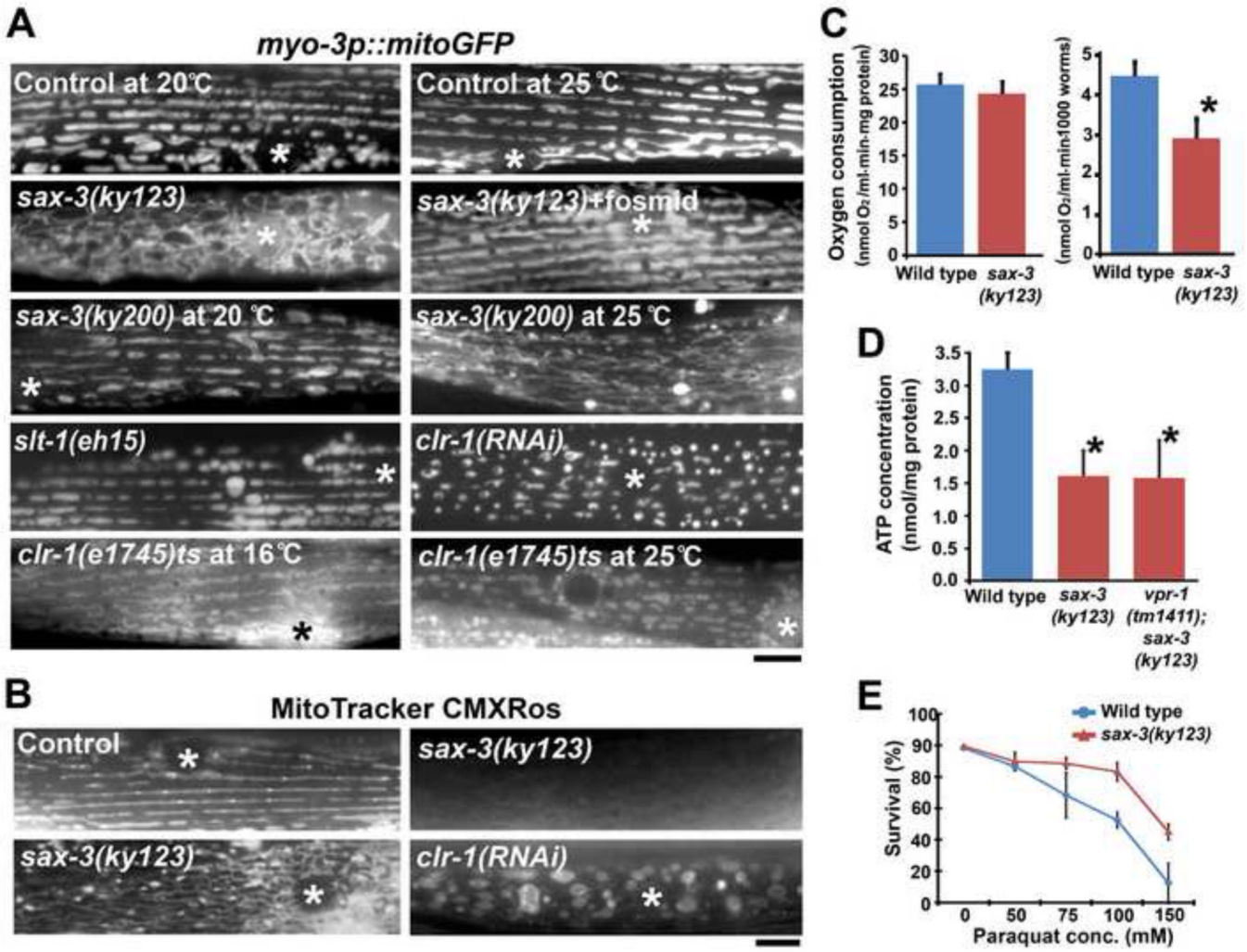

Figure 6. *sax-3* Robo and *clr-1* Lar-like receptor mutant phenotypes

(A) Muscle mitochondrial networks in wild-type control and mutant hermaphrodites. Fosmid indicates expression of a transgene containing the *sax-3* genomic locus. *sax-3(ky200)ts* mutants were shifted to the non-permissive temperature (25°C) at the L1 stage and scored in 1 day adults. *clr-1(e1745)ts* mutants were shifted to the non-permissive temperature (25°C) in young adults and scored 12 hours later. Asterisks indicate nucleus. Bar, 5 μm.

(B) MitoTracker CMXRos staining of live muscles. Asterisks indicate nucleus. Bar, 5 μm.

(C) Oxygen consumption rates of wild type and *sax-3* mutant 1 day old adults. Consumption rates were normalized to protein content (left) or worm number (right). *, $P < 0.005$ compared to wild type. Error bars represent SD.

(D) ATP concentration in wild-type and mutant hermaphrodite extracts. *, $P < 0.001$ compared to wild type. Error bars represent SD.

(E) Paraquat sensitivity in wild-type and *sax-3(ky123)* hermaphrodites. Error bars represent SD.

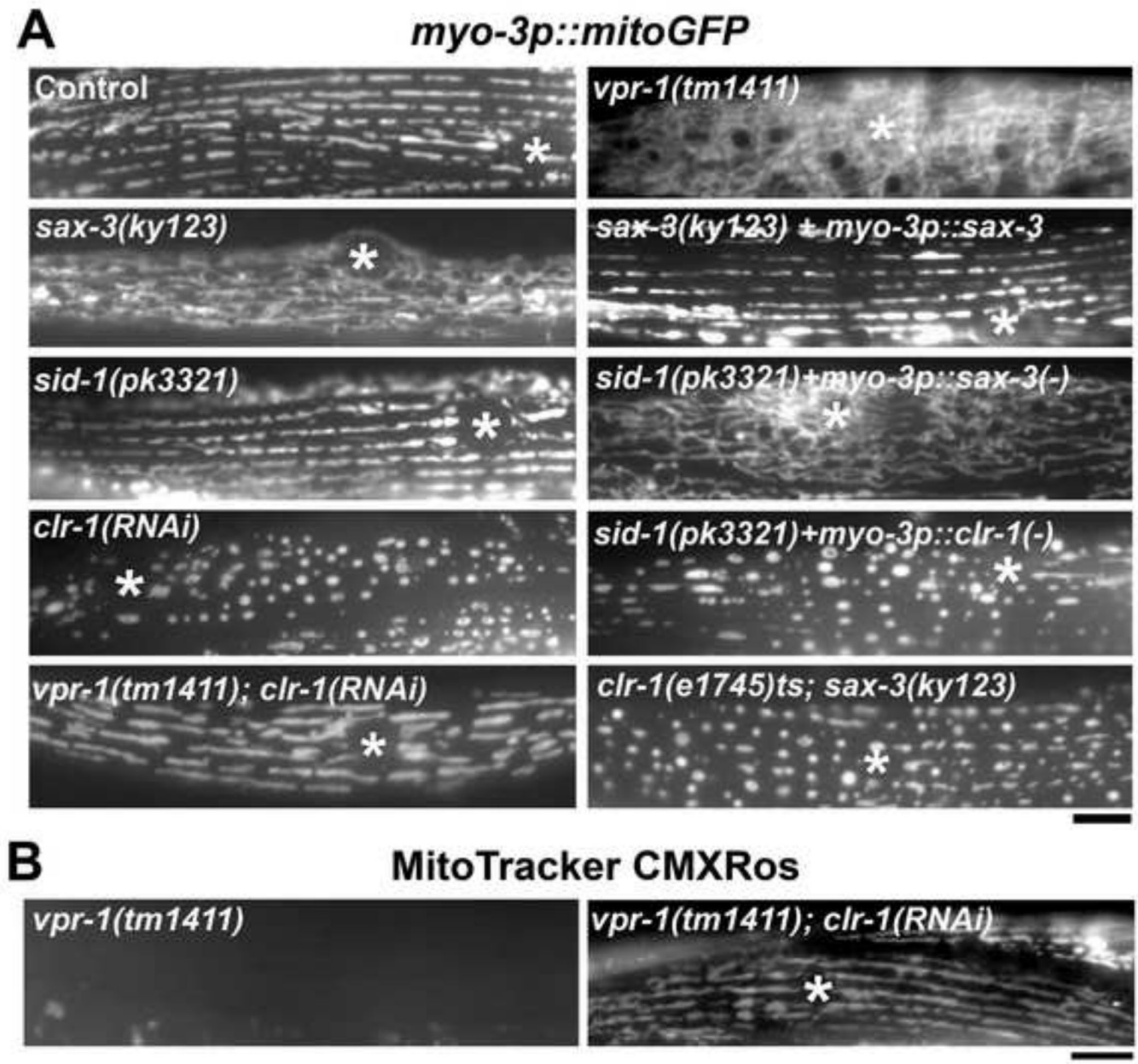

Figure 7. *sax-3* Robo and *clr-1* Lar site of action and signaling hierarchy

(A) Muscle mitochondrial networks in wild-type control and mutant hermaphrodites. The *myo*-3 promoter was used to drive *sax-3* cDNA, *sax-3* antisense/sense RNAi (−), or *clr-1* antisense/sense RNAi (−) expression specifically in body wall muscle. *sid-1(pk3321)* mutants are defective for systemic RNAi, but cell autonomous RNAi occurs normally. *clr-1(e1745)ts; sax-3(ky123)* mutants were scored at the non-permissive temperature. Unlike mitochondria in *vpr-1(tm1411); clr-1* RNAi mutants, mitochondria in *clr-1(e1745)ts; sax-3(ky123)* mutants fail to elongate on the I-bands. Asterisks indicate nucleus. Bar, 5 μm. (B) MitoTracker CMXRos staining of live muscles. Asterisks indicate nucleus. Bar, 5μm.

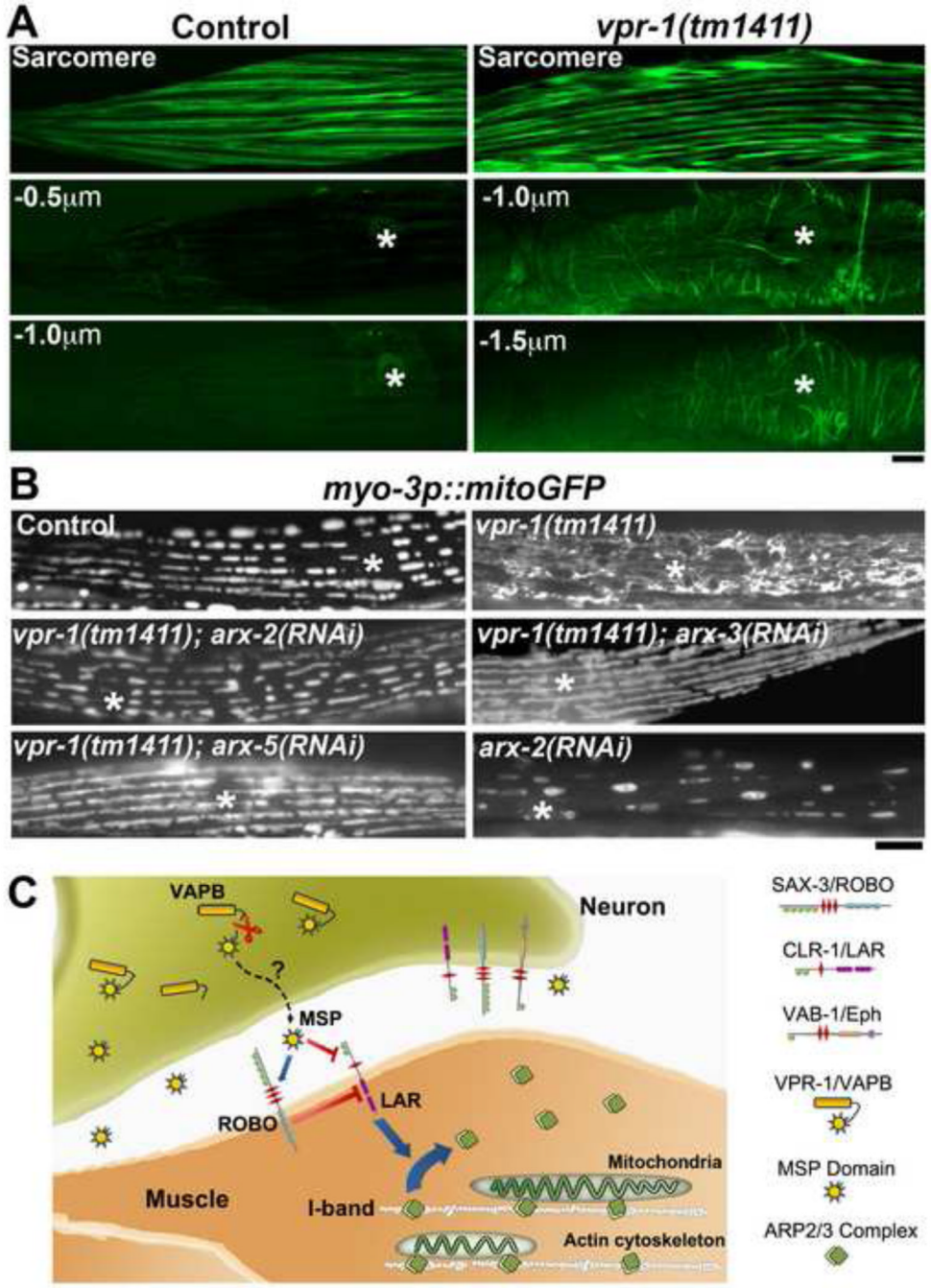

Figure 8. VAP regulation of Arp2/3 complex activity and working model

(A) Filamentous actin distribution in wild-type and *vpr-1* mutant muscle, observed using muscle-specific expression of the moesin actin binding domain fused to GFP. Deconvolved images from axial scans are shown. Belly panels are shown with distances beneath the sarcomere or myofilaments. Asterisks indicate nucleus. Bar, 5 μm.

(B) Muscle mitochondrial networks in wild-type control and mutant/RNAi hermaphrodites. Asterisks indicate nucleus. Bar, 5 μm.

(C) Working model. See text for details.